symmetry

MDPI

Article

Experimental Investigation on the Effectiveness of EB-CFRP Confinement of Elliptical Concrete Columns

Zine El Abidine Benzeguir [1], Omar Chaallal [1], Ahmed Godat [2,*] and Rami A. Hawileh [3]

[1] Department of Construction Engineering, École de Technologie Supérieure (ÉTS), Université du Québec, Montreal, QC H3C 1K3, Canada; zine-el-abidine.benzeguir@etsmtl.ca (Z.E.A.B.); omar.chaallal@etsmtl.ca (O.C.)
[2] Department of Civil Engineering, College of Engineering and Information Technology, Ajman University, Ajman P.O. Box 346, United Arab Emirates
[3] Department of Civil Engineering, College of Engineering, American University of Sharjah, Sharjah P.O. Box 26666, United Arab Emirates; rhaweeleh@aus.edu
* Correspondence: a.godat@ajman.ac.ae

Abstract: This paper presents the results of an experimental study involving 20 tests performed on elliptical concrete columns confined with externally bonded carbon fiber-reinforced polymer (EB-CFRP) laminates. The study aimed to evaluate the effects of elliptical aspect ratio (A/B) as well as confinement rigidity (number of EB-FRP layers) on confinement effectiveness. The experimental program consisted of one series of control concrete columns (unstrengthened) and three additional series, each one strengthened with one, two and three layers of EB-CFRP sheets, respectively. Furthermore, each series considered five elliptical aspect ratios (A/B) ranging from 1.0 to 1.6. Following compressive concentric tests until failure, the results were analyzed to characterize the confinement level with an increasing number of EB-CFRP layers as a function of the elliptical aspect ratio. The results show considerable enhancements in compressive strength and in the ductility of the confined columns. Furthermore, this improvement is amplified as the number of EB-CFRP layers increases, indicating a proportional relationship between the compressive strength and the number of CFRP layers. It is found that the ultimate strength of EB-CFRP-confined columns with three layers reached up to 130% compared to the control specimens. However, increasing the elliptical aspect ratio reduced the compressive strength and ductility of confined columns. This study investigated the relation between the CFRP hoop and axial strains and the elliptical aspect ratios. Moreover, through comparison, the results reveal that the prediction models proposed by the Canadian standards S806-12 and S6-19 do not capture the negative effect of the elliptical aspect ratio in confined concrete columns.

Keywords: elliptical concrete column; aspect ratio; confinement; strengthening; EB-CFRP; number of layers; compressive strength; stress–strain

Citation: Benzeguir, Z.E.A.; Chaallal, O.; Godat, A.; Hawileh, R.A. Experimental Investigation on the Effectiveness of EB-CFRP Confinement of Elliptical Concrete Columns. *Symmetry* **2024**, *16*, 1595. https://doi.org/10.3390/sym16121595

Academic Editor: Lei Jiang

Received: 2 October 2024
Revised: 4 November 2024
Accepted: 12 November 2024
Published: 29 November 2024

1. Introduction

Exposed reinforced concrete (RC) structures and, in particular, bridge elements suffer serious deterioration under severe climatic conditions due to the gradual increase in the regulatory loads of heavy trucks and the increasing frequency of their passage. Strengthening techniques using externally bonded fiber-reinforced polymer (EB-FRP) composites are increasingly used because of their efficiency, cost-effectiveness, speed, and ease of application compared to conventional techniques using steel plates. Confining concrete columns with EB-FRP to enhance their compressive strength and seismic performance are examples of this evolving technique.

Numerous experimental studies have been carried out on the confinement of concrete columns using various techniques. Concrete-filled steel tubes [1], concrete-filled FRP tubes [2–6], concrete-filled both FRP and steel tubes [7], prefabricated textile-reinforced concrete [8–10], EB-FRP composites using wet lay-up [11–23], and FRP ropes [24] are

examples of such strengthening techniques. In addition, many numerical studies simulating confined concrete columns have also been carried out [1,17,25–29].

The use of elliptical tube-confined concrete columns is a technique for obtaining an elliptical column section using an FRP elliptical tube as formwork. In addition to concrete, expanding cement is also used, which will create a post-tensioning action with the old concrete during column jacketing [3]. This technique replaces steel with FRP tubes to take advantage of the light weight of the FRP material and its resistance properties in severe environments, such as corrosion resistance. The FRP has excellent ductility when used in seismic retrofitting [6]. The second ovalization technique for the EB-FRP confinement of concrete columns involves, firstly, full reshaping of the concrete cross-section from square to circular (Figure 1a) or from rectangular to elliptical (Figure 1b) by jacketing the old concrete. The newly prepared columns can then be confined using wet lay-up EB-FRP laminates. This technique is the most widely used in practice for existing concrete structural elements. Another technique, which is rarely used, consists of slightly curving the four flat sides of the concrete column and rounding the corners with a given radius (r_c) instead of modifying the full cross-section (Figure 1c). This technique was implemented in some experimental research studies [30–32]. In this technique, the new concrete or mortar used must have a compressive strength at least equal to that of the existing column to avoid premature failure of the FRP/concrete interfacial layer, which may lead to crushing of the columns.

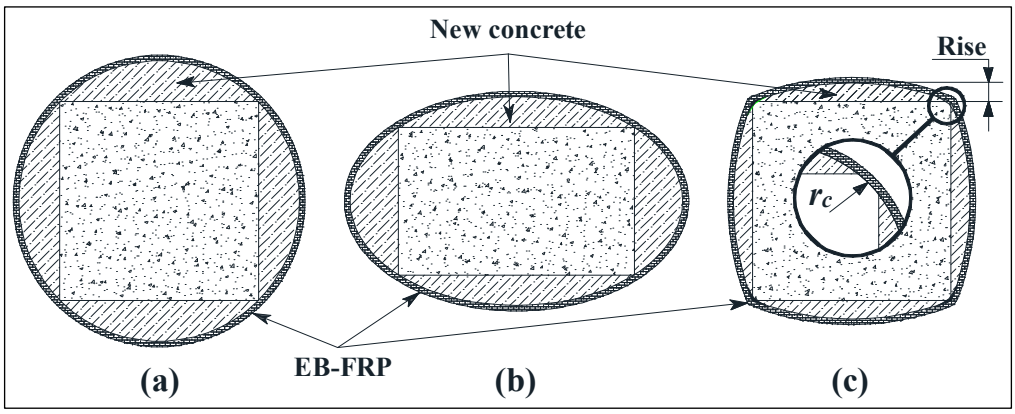

Figure 1. Section ovalization for EB-FRP confinement of rectangular or square concrete column: (**a**) square to circular cross-section; (**b**) rectangular to elliptical cross-section, and (**c**) rounding corners of cross-section.

Teng and Lam [12] carried out an experimental study on 20 specimens with four aspect ratios of major to minor axes (A/B from 1.0 to 2.5) confined with EB-CFRP laminates of different rigidities. The results of the study revealed that the compressive strength of confined concrete is proportional to CFRP rigidity, but inversely proportional to aspect ratio. In addition, they also showed that the effectiveness of confinement decreases as the aspect ratio A/B increases. To avoid the phenomenon of decreasing compressive strength with increasing aspect ratio A/B, the authors suggested consideration of an effective confinement pressure (f_{lF}) using a reduction factor that accommodates the elliptical aspect ratio effect.

Yan and Pantelides [3] evaluated large-scale columns of almost 1.0 m height confined with elliptical FRP tubes using carbon and glass fibers. Two concrete types, expansive cement concrete and non-shrink cement concrete, were used to modify three types of cross-sectional column shapes from square to circle and from rectangle to ellipse with two aspect ratios, A/B = 2 and 3. Note that to confirm confinement activation before loading, FRP deformation was measured after cement expansion in the FRP formwork. The axial strain reached around 0.002, 0.0018, and 0.0015 mm/mm for the circular (A/B = 1.0), elliptic with A/B = 2.0, and elliptic with A/B = 3.0 specimens, respectively. The authors concluded that the confinement effect of non-bonded FRP laminates combined with expansive cement concrete is superior to that with no-shrink cement concrete and a bonded FRP jacket. They

also confirmed that the optimal cross-sectional shape for FRP confinement is the circular cross-section.

The experimental investigation of Zeng et al. [19] considered 33 EB-CFRP-confined columns. FRP rigidity as well as confinement schemes (full and partial wrapping) were the study parameters. The results showed a considerable increase in deformation and compressive strength capacity in the elliptical confined columns compared to the square ones. As the partial wrapping confinement schemes and the spacing of the FRP strips increased, the ultimate capacity decreased. The results also revealed that the combination of ovalization with partial wrapping schemes, which saves 50% of the EB-CFRP material, is comparable and even more effective than confined square columns with full wrapping schemes.

The effect of high concrete strength (72.4 MPa) on the confinement of concrete columns with the elliptical FRP tube technique was examined by Chen et al. [4]. The elliptical aspect ratio A/B was also considered as a parameter, ranging from 1.0 to 2.0, as well as the FRP rigidity considering carbon and glass materials. The authors concluded that the stress capacities of elliptical confined concrete columns were enhanced by increasing the FRP rigidity (number of layers). The axial behavior of the columns was negatively impacted by the rising sectional aspect ratio and the usage of high-strength concrete due to the irregular distribution of FRP confining pressure.

On the other hand, a comparison of experimental test results with the predictions of current codes of practice and design guidelines to assess their accuracy seems to indicate that the current guidelines do not capture the effect of the elliptical aspect ratio. It has been found that they use the same models for predicting the axial compressive strength of both circular and elliptical columns. As reported by Zeng et al. [19], the CNR-DT200R1 [33] design equation overestimates the ultimate axial stress of confined specimens, and the *fib*-TG9.3-19 [34] prediction model exaggerates the ultimate axial strain of concrete partially confined with FRPs.

In the present study, the authors carried out an experimental investigation using confined concrete columns with the wet lay-up EB-CFRP technique. The EB-CFRP technique was selected because of its frequent use for existing columns requiring strengthening. As explained above, it represents a better option for rehabilitation or seismic upgrading than the elliptical tube-confined concrete column technique, which remains a column design of choice. Furthermore, the present experimental study aims to evaluate the behavior of concrete columns confined with EB-CFRP as a function of the following varied aspects: (1) elliptical aspect ratio (A/B) and (2) EB-CFRP rigidity (number of layers). In addition, a comparison of the obtained experimental results with the predictions of current design codes is also presented in this study. The confinement of elliptical columns develops non-uniform CFRP stress distribution across the cross-section due to the varying curvature along the major and minor axes. This introduces unique symmetry-related challenges to understand the behavior of confinement effectiveness. Furthermore, experimental tests on CFRP-confined elliptical columns involve symmetrical loading conditions (e.g., concentric loading), which require evaluating symmetrical wrapping patterns around the elliptical shape to optimize the structural performance of CFRP-confined columns.

2. Research Significance

Research studies on confined concrete columns using the EB-FRP technique with various elliptical aspect ratios are very few and of limited scope. The most studied parameters in the literature are the modification of a square cross-section into a circular one using different circularization methods, as well as the use of various strengthening configurations (continuous vs. discontinuous). However, confinement depends mainly on the elliptical aspect ratio because its effectiveness is related to the FRP pressure distribution around the elliptical shape and also to the rigidity of EB-FRP sheet (number of layers). The present study is an attempt to understand the phenomenon of the non-uniform pressure distribution of EB-FRP around the cross-section with respect to the elliptical aspect ratio (A/B). It also provides additional experimental data and recommendations for researchers and

practical engineers to express the relationship between variation in compressive strength and elliptical aspect ratio.

3. Confinement Mechanism

The confinement of concrete columns is required to (1) repair damage (cracking or steel corrosion); (2) increase load-bearing capacity (change in initial purpose); or (3) increase ductility (seismic upgrading). It is also useful to confine an existing concrete column to favor a sequence of failure modes, such as the concept of a beam yielding before a column, known as the strong column–weak beam concept. The confinement mechanism for concrete columns consists of applying lateral pressure around the section with FRP laminates to restrain the lateral expansion of concrete (Figure 2).

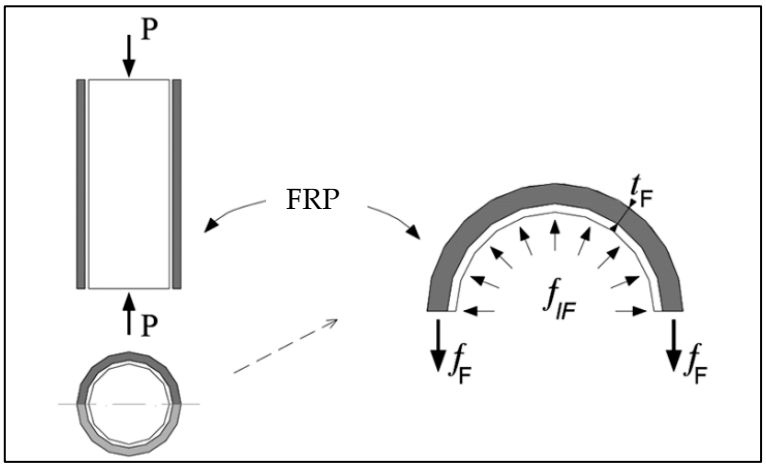

Figure 2. Confinement mechanism with FRP in circular column.

Concrete column cross-sections are square, rectangular, or circular, but rarely oval or elliptical. Confinement depends mainly on the geometry of the column cross-section and is more effective when the cross-section is circular. The confinement pressure is uniform for a circular column, while it is much higher at the corners than on the flat sides of a rectangular section, resulting in partial and non-uniform confinement of the section and favoring the premature rupture of EB-FRP (Figure 3). The limited confinement performance of square or rectangular columns is attributed to non-uniform confinement around the section, in contrast to the circular section, where it is uniformly distributed and most effective.

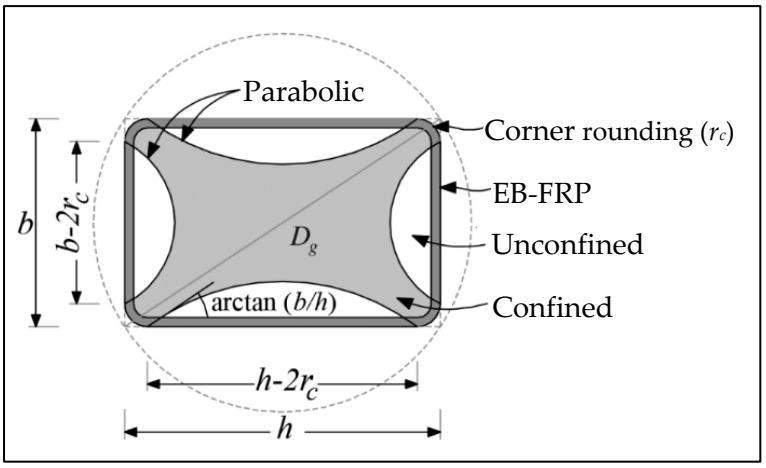

Figure 3. Confinement with FRP in rectangular column.

Before confining square or rectangular sections with the EB-FRP technique, the standards recommend rounding the four corners of the column to attenuate stress concentra-

tions and delay premature fiber rupture in these areas. To that end, a minimum radius (chamfer radius) is specified ($r_c \geq 20$ mm for CSA-S806-21 [35] and $r_c \geq 35$ mm for CSA-S6-19 [36] (Figure 3). According to Teng and Lam (2002) [12], the effectiveness of square or rectangular cross-section confinement is proportional to the rounding radius r_c. However, the rounding radius can be limited by the presence of longitudinal reinforcing bars at the four corners. It can be deduced that section ovalization remains the most efficient alternative for optimizing EB-FRP-confined concrete columns.

4. Experimental Program

The experimental program involved 20 tests performed on an elliptical section to study the behavior of confined columns with EB-CFRP laminates. The investigated parameters included (1) the influence of the elliptical aspect ratio (A/B) and (2) the influence of EB-CFRP rigidity (number of CFRP layers). This section presents the following details: (a) specimen details; (b) materials used; (c) strengthening procedure; and (d) test setup and instrumentation.

4.1. Specimen Details

Figure 4 presents a typical cross-section of a confined specimen. The specimen cross-section is defined according to elliptical properties. The major vertices of the specimen lie along the major axis with length A (A = 2a), and the minor vertices occur along the minor axis with length B (B = 2b). It can be mentioned that the cross-section area was kept identical for all elliptical-shape specimens. In addition, the cross-section area for circular-section (A = 212 mm^2) specimens was approximately equal to the elliptical-section (A = 208 mm^2) specimens.

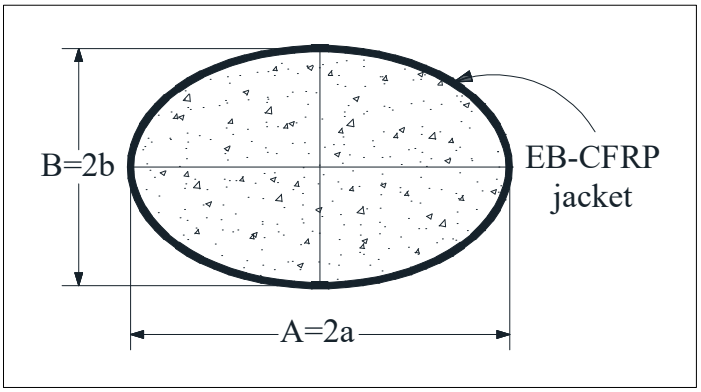

Figure 4. Typical cross-section of elliptical specimen.

The details of all specimens and the test setup are presented in Figure 5 and Table 1. The 20 column specimens are divided into four series: unstrengthened (control) and those strengthened with one, two, or three layers of EB-CFRP laminates, respectively. They were prepared from five different batches of concrete, as provided in Table 1. Note that the concrete columns were not reinforced with internal steel. The objective of the present study was to evaluate confinement effectiveness as influenced by (1) the elliptical shape aspect ratio and (2) the axial rigidity of the EB-FRP (number of layers). To that end, each series included one circular specimen (A/B = 1.0) and four elliptical ones with aspect ratios A/B of 1.3, 1.4, 1.5, and 1.6, respectively. Dimensional details of each specimen, including major and minor vertices, number of CFRP layers, thickness of CFRP laminates, and concrete compressive strength, are detailed in Table 1.

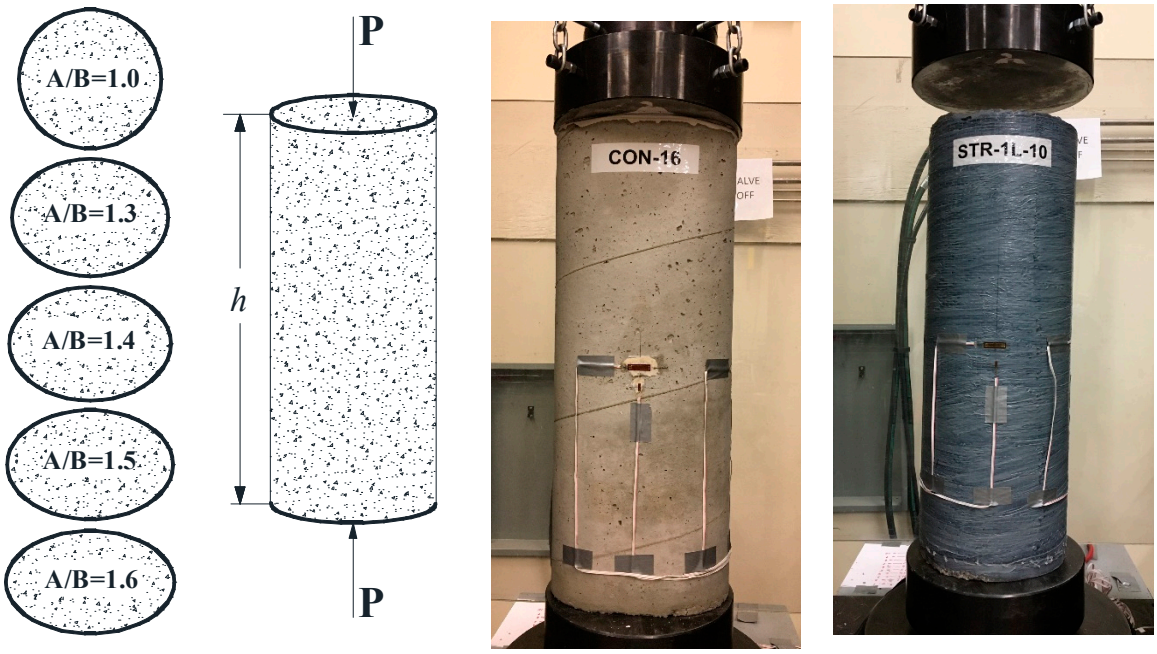

Figure 5. Details of tested specimens.

Table 1. Test matrix.

Specimen	Series	A (mm)	B (mm)	Aspect Ratio A/B	h (mm)	CFRP Layers	t_{FRP} (mm)	f'_{ccyl} (MPa)
Con-1.0	Serie 1 Unstrengthened (Control)	212	212	1	624	-	-	35.8
Con-1.3		233	179	1.3	623	-	-	35.8
Con-1.4		240	173	1.4	627	-	-	35.8
Con-1.5		246	167	1.5	625	-	-	35.8
Con-1.6		251	157	1.6	626	-	-	30.2
STR-1L-1.0	Serie 2 Strengthened 1 layer	212	212	1	624	1	0.13	37.5
STR-1L-1.3		233	179	1.3	623	1	0.13	37.5
STR-1L-1.4		240	173	1.4	627	1	0.13	37.5
STR-1L-1.5		246	167	1.5	625	1	0.13	37.5
STR-1L-1.6		251	157	1.6	626	1	0.13	30.2
STR-2L-1.0	Serie 3 Strengthened 2 layers	212	212	1	624	2	0.26	40.2
STR-2L-1.3		233	179	1.3	623	2	0.26	40.2
STR-2L-1.4		240	173	1.4	627	2	0.26	40.2
STR-2L-1.5		246	167	1.5	625	2	0.26	40.2
STR-2L-1.6		251	157	1.6	626	2	0.26	30.2
STR-3L-1.0	Serie 4 Strengthened 3 layers	212	212	1	624	3	0.39	36.8
STR-3L-1.3		233	179	1.3	623	3	0.39	36.8
STR-3L-1.4		240	173	1.4	627	3	0.39	36.8
STR-3L-1.5		246	167	1.5	625	3	0.39	36.8
STR-3L-1.6		251	157	1.6	626	3	0.39	30.2

In Table 1, the specimens are designated and labeled as follows: Con for a control specimen; STR for a strengthened (confined) specimen followed by 1L, 2L, and 3L for, respectively, one, two, and three layers of EB-CFRP. The last term in the nomenclature indicates the value of the aspect ratio A/B (1.0, 1.3, 1.4, 1.5, or 1.6). For instance, specimen STR-2L-1.5 is a confined column with two layers of CFRP laminates and has an aspect ratio of 1.5.

4.2. Materials

The same concrete mix design was used for all specimens, and it was fabricated in the laboratory. The average concrete compressive strength ($f'_{c\ cyl}$), presented in Table 1, was obtained by performing three tests on cylinders according to the ASTM-C39/39-21 (2021) [37] standard on the test day. Unidirectional CFRP sheets were used to confine all specimens. Table 2 presents the mechanical properties of the CFRP sheets as well as the epoxy matrix used to impregnate and bond the sheet, as provided by the manufacturer.

Table 2. Mechanical properties of CFRP fabric and epoxy matrix.

Material	Properties	Value
Laminate	Tensile strength, f_{FRPu} (MPa)	3450
	Modulus of elasticity, E_{FRP} (GPa)	230
	Elongation at break, ε_{FRPu} (%)	1.5
	Thickness, t_{FRP} (mm)	0.13
Epoxy	Tensile strength, f_{FRPu} (MPa)	30
	Modulus of elasticity, E_{FRP} (GPa)	4.5
	Elongation at break, ε_{FRPu} (%)	2.0

4.3. Strengthening Procedure

The concrete surface was first sandblasted to remove irregular surfaces and to clean off particles and impurities to achieve an adequate surface profile index before the application of EB-CFRP laminates. Its length was prepared, including the number of layers (circumference of the elliptical specimen times the number of layers) and an additional 300 mm length for overlapping, as recommended by the manufacturer. An epoxy resin coating was applied directly onto the concrete surface using a trowel and a paint roller. The CFRP sheets (one, two, or three layers) were then bonded around the specimen section to confine the column. At the same time, the epoxy was squeezed throughout the roving of the CFRP sheets with a special roller to saturate the fibers and to remove trapped air pockets and excess epoxy at the concrete/epoxy and epoxy/CFRP sheet interfaces. A thin layer of epoxy resin was left at the end of the last CFRP layer to act as a protective screen for the fibers. Note that the unidirectional carbon fibers were applied perpendicularly to the longitudinal axis of the specimen.

4.4. Test Setup and Instrumentation

The specimens were subjected to monotonic concentric compression loading under displacement control conditions at a rate of 0.4 mm/min until failure in conformity with ASTM-C39/39-21 [37]. A comprehensive and carefully engineered measuring device was mounted to instrument 5 mm long strain gauges around the specimen circumference at the columns' mid-height, as shown in Figure 6. The figure shows the instrumentation on the confined specimens, where the horizontal orientation is represented by (H), which measures the strain in the circumferential direction in both the control and confined specimens. The vertical orientation is represented by (V), which measures the vertical strain along the column axis direction. However, there are neither strain gauges H3 and H4 in the circular control specimens (unconfined column), nor gauges H3, H4, H5, H6, H7, and H8 in the elliptical control specimens. Changes in the overall height of the columns were also measured with linear-variable differential transducers (LVDTs). It should be mentioned that the non-uniform (top-end) face of all specimens was leveled with a high-strength self-leveling compound (dry stone) to achieve a uniformly distributed applied axial load during the test.

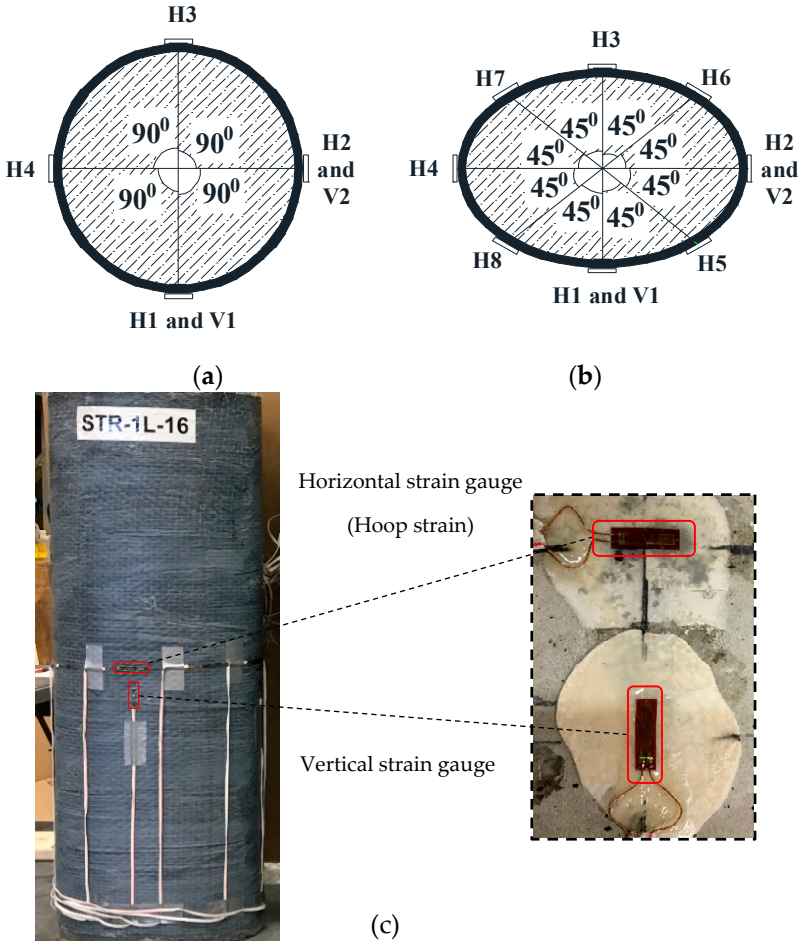

Figure 6. Strain gauges' locations around the specimen section: (**a**) circular specimen, (**b**) elliptical specimen, and (**c**) strain gauges' orientation.

5. Experimental Test Results

Table 3 presents the experimental test results. The obtained test results include the compressive strength of the concrete cylinders ($f'_{c\,cyl}$), the maximum attained loading capacity (P_{max}), the gain in load capacity due to EB-CFRP confinement (load gain), the compressive concrete strength (f'_c), the compressive confined concrete strength (f'_{cc}), the gain in compressive strength (f'_{cc}/f'_c), the axial maximum displacement (ΔL), the maximum horizontal hoop strain (ε_H), the maximum vertical strain (ε_V), and the specimen failure mode. The following sections present relevant results in terms of (1) failure mode by visual inspection; (2) load-carrying capacity, (3) displacement response, (4) concrete compressive strength, and (5) vertical and horizontal strain response curves.

Table 3. Summary of test results.

Specimen	$f_c cyl$ (MPa)	P_{max} (kN)	Load Gain (%)	f_c (MPa)	f_{cc} (MPa)	f_{cc}/f_c	ΔL (mm)	ε_H (μm/m)	ε_V (μm/m)	Failure Mode
Con-1.0	35.8	1059	-	30.1	-	-	1.9	402	2711	
Con-1.3	35.8	1016	-	31.1	-	-	2.1	918	2306	
Con-1.4	35.8	1039	-	31.9	-	-	2.1	741	2904	CC
Con-1.5	35.8	1023	-	31.6	-	-	2	734	1289	
Con-1.6	30.2	820	-	26.5	-	-	2.3	6586	3958	
STR-1L-1.0	37.5	1433	35	30.1	40.7	1.35	9	13,811	8139	
STR-1L-1.3	37.5	1252	23	31.1	38.3	1.23	7.6	12,482	9969	CFRP
STR-1L-1.4	37.5	1150	11	31.9	35.3	1.11	5.5	11,756	5361	rupture/
STR-1L-1.5	37.5	1061	4	31.6	32.8	1.04	2.5	1397	3058	CC
STR-1L-1.6	30.2	1099	34	26.5	35.5	1.34	9.2	13,849	17,268	

Table 3. *Cont.*

Specimen	$f_c cyl$ (MPa)	P_{max} (kN)	Load Gain (%)	f_c' (MPa)	f_{cc}' (MPa)	f_{cc}'/f_c'	ΔL (mm)	ε_H (μm/m)	ε_V (μm/m)	Failure Mode
STR-2L-1.0	40.2	1999	89	30.1	56.8	1.89	15.3	15,515	29,740	
STR-2L-1.3	40.2	1696	67	31.1	51.9	1.67	12.7	13,239	21,330	CFRP
STR-2L-1.4	40.2	1682	62	31.9	51.6	1.62	13.8	17,530	15,655	rupture/
STR-2L-1.5	40.2	1553	52	31.6	48	1.52	13.7	16,324	22,234	CC
STR-2L-1.6	30.2	1340	63	26.5	43.3	1.63	11.8	12,177	16,937	
STR-3L-1.0	36.8	2513	137	30.1	71.4	2.37	22.4	15,760	31,313	
STR-3L-1.3	36.8	1974	94	31.1	60.4	1.94	16.9	15,732	15,432	CFRP
STR-3L-1.4	36.8	1832	76	31.9	56.2	1.76	14.3	15,915	15,440	rupture/
STR-3L-1.5	36.8	1661	62	31.6	51.4	1.62	13.5	15,910	15,431	CC
STR-3L-1.6	30.2	1582	93	26.5	51.1	1.93	17.4	17,800	13,092	

$f'_{C\ cyl}$ = cylinder compressive strength of concrete. ΔL = Change in the overall height of column (specimen's shortening). $\varepsilon_{H=}$ maximum circumferential hoop column strain (horizontal). $\varepsilon_{V=}$ maximum axial column strain (vertical). CC = concrete crushing.

5.1. Failure Mode

The failure mode of all control specimens was, as expected, a well-defined fracture pattern, as shown in Figure 7a. According to standard test methods for compressive strength on cylindrical concrete specimens, the failure was of type 2, which means a well-formed cone on one end with vertical cracks running through the cap and no well-defined cone on the other end [37]. In contrast, crack development in confined specimens could not be observed during the tests due to the presence of continuous EB-CFRP sheets. However, immediately after the tests, the CFRP sheets were removed to observe the fracture patterns, which are shown in Figure 7b–d. The deformation at failure was obtained at the specimen failure.

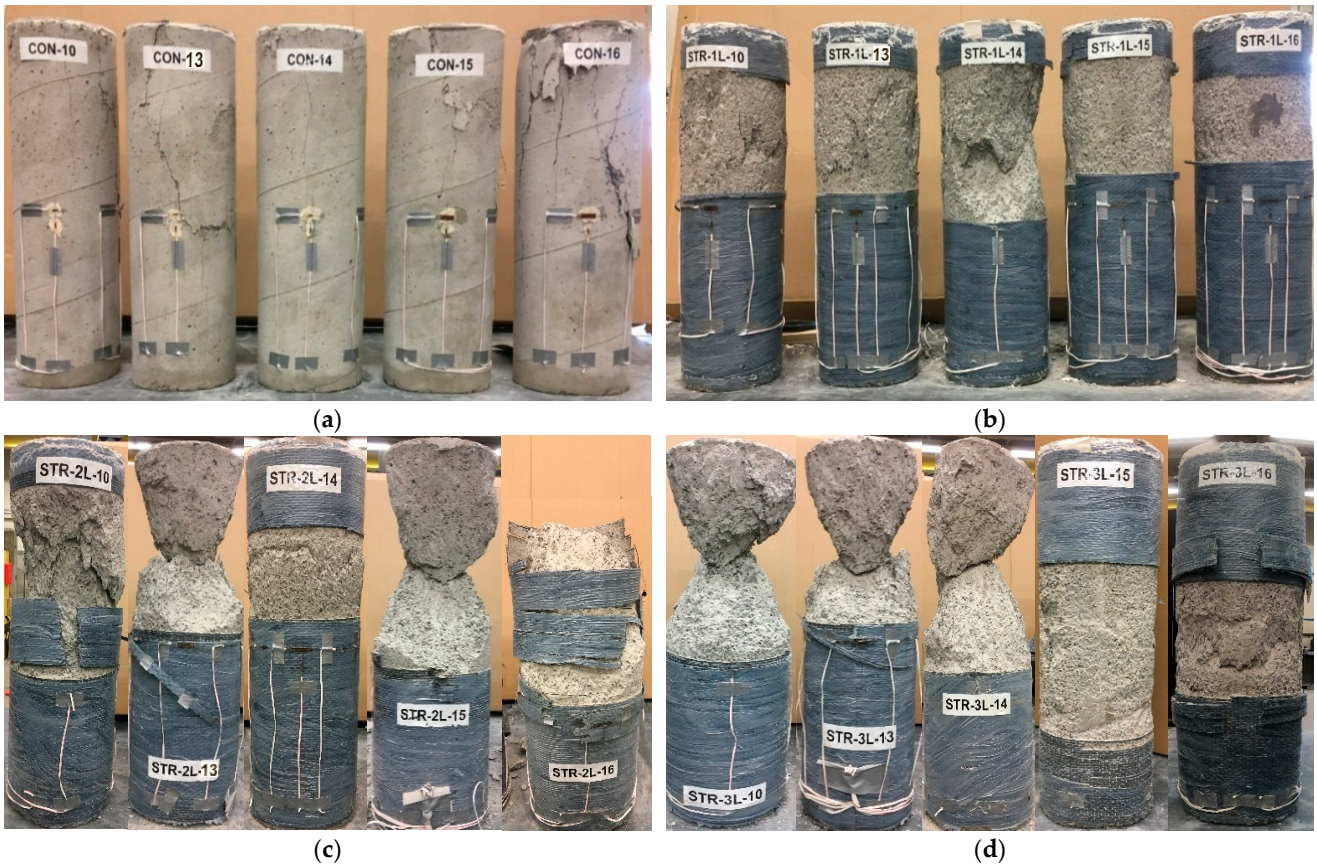

Figure 7. Typical failure mode of specimens: (**a**) cracking patterns for control specimens; (**b**) confined specimens with 1 CFRP layer; (**c**) with 2 CFRP layers; and (**d**) with 3 CFRP layers.

As predicted, the failure mode of all confined specimens, whatever the aspect ratio A/B, was by rupture of the CFRP jacket accompanied by concrete crushing (Figure 7b–d). Note that all confined specimens featured a failure mechanism similar to that reported by Teng et Lam [12] and Teng et al. [17]. The failure mechanism of concrete initiates when the concrete reaches its compressive strength; cracks expand quickly and the CFRP is unable to prevent the concrete's crushing. When the number of CFRP layers is increased, the column can withstand higher applied loads because CFRP provides a restraining force and increases ductility. As loading increases, the concrete core gradually fails, and cracks propagate outward until the sudden rupture of CFRP layers. Here, with increasing load, the ultimate concrete strain ε_{cu} in confined specimens was reached, resulting in crushing, whereas at the ultimate load, pulverization of the concrete occurred, leading to the separation of the specimen into two parts. This is also true in the confined specimens with two or three CFRP layers (Figure 7c,d). In the specimens with three CFRP layers, a sudden fracture of the CFRP jacket followed by a loud explosive noise and random volatility of the pulverized concrete was observed. This may indicate that CFRP contributes to ultimate strength despite concrete crushing. During the tests of confined specimens, no signs of rupture were observed until the sudden break. After the removal of the CFRP sheets, a thin layer of concrete remained attached to the sheets, indicating the effectiveness of the epoxy in bonding the CFRP to the concrete. No difference was observed in the rupture mode as the aspect ratio A/B or the number of confinement layers increased.

5.2. Load-Carrying Capacities

Figure 8 presents the loading versus the increase in the aspect ratio (A/B) and EB-CFRP rigidity for each series. The maximum attained load in the control specimens reached 1059 kN for circular Con-1.0 and decreased when increasing the A/B ratio by 23% in specimen Con-1.6. In contrast, in the confined specimens, the highest recorded load was 2513 kN in specimen STR-3L-1.0, representing a 137% increase with respect to the corresponding control specimen. The histograms in Figure 8 show a significant increase in the maximum attained load on each series with the same aspect ratio (A/B) as the number of EB-CFRP layers increases. This is consistent with findings reported in the literature [6] and can be attributed to the increase in CFRP rigidity, which enhanced the tensile force provided by the FRP fibers and hence the confinement pressure, as also expressed by the model code. Indeed, according to the Canadian highway bridge design code [36], the confinement pressure (f_{lF}) prediction model, which governs the confined compressive strength $\left(f'_{cc}\right)$, is proportional to EB-FRP rigidity, as expressed in Equation (1). Moreover, the loading capacity (P_r) is directly proportional to the compressive strength $\left(f'_{cc}\right)$ of the confined concrete (Equation (3)), as follows:

$$f_{lF} = \frac{2t_F \varnothing_F E_F \varepsilon_{Fu}}{D_g} \quad (1)$$

$$f'_{cc} = f'_c + 2f_{lF} \quad (2)$$

$$P_r = 0.80\left[\alpha_1 \varnothing_c f'_{cc}\left(A_g - A_s\right) + \varnothing_s f_y A_s\right] \quad (3)$$

where t_F, φ_F, E_F, and ε_{Fu} are the thickness, resistance factor taken as 0.75, elastic modulus, and ultimate strain of FRP laminates, respectively; D_g is the column diameter; A_g and A_s are the gross section area of the column and longitudinal reinforcement area, respectively; α_1 is an eccentricity reduction factor; φ_c and φ_s are strength reduction factors for concrete and reinforcing steel taken as 0.65 and 0.85, respectively.

In the other series, the gain in load decreased as the aspect ratio increased. In fact, the increase was 137% in STR-3L-1.0 in the first series (A/B = 1.0) and decreased to 94%, 76%, and 62% for A/B = 1.3, 1.4, and 1.5, respectively. The trend of the gain in load increased as the CFRP rigidity increased. For instance, the gain in specimens of the first series (A/B = 1.0) was 35%, 89%, and 137% for one, two, and three layers, respectively, whereas for the series

(A/B = 1.6), it was 34%, 63%, and 93%, respectively (Figure 8 and Table 3). This clearly demonstrates and corroborates the observation that the aspect ratio (A/B) significantly impacts the EB-FRP confinement effectiveness.

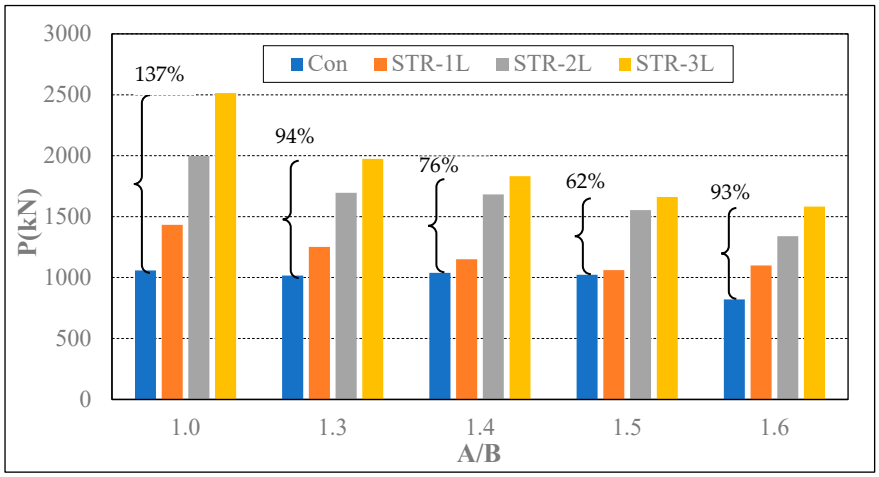

Figure 8. Maximum load versus increasing aspect ratio (A/B) and EB-CFRP rigidity.

Based on Figure 8, the results for aspect ratio A/B = 1.0 compared to those with A/B = 1.6 are self-explanatory in emphasizing the difference in confinement behavior between circular and elliptical columns, regardless of the rigidity of EB-CFRP confinement. This contrasts with the predictive model of the Canadian standard CSA-S806-21 [35], which specifies different prediction models for rectangular and circular sections. However, the design standard implements an identical model for circular and elliptical sections (Equation (5)). This may have a negative effect on the capacity of confined concrete columns with EB-FRP calculated using the guidelines as follows:

$$f'_{cc} = 0.85f'_c + k_1 k_c f_{lF} \tag{4}$$

$$k_c = \begin{cases} 1.0 \text{ for circular and oval section} \\ 0.4 \quad \text{for rectangular section} \end{cases} \quad \text{for rectangular section} \tag{5}$$

$$k_1 = 6.7(k_c f_{lF})^{-0.017} \tag{6}$$

5.3. Displacement Response

The axial displacement (ΔL = specimen shortening) corresponding to the maximum load P_{max} (Table 3) was practically the same in all control specimens regardless of aspect ratio variation. However, it increased with (a) specimen confinement; (b) the number of EB-CFRP layers; and (c) decreasing aspect ratio. In fact, the axial displacements increased from 2 mm in control specimen Con-1.5 to 2.5 mm in confined specimen STR-1L-1.5 and to 13.5 mm in confined specimen STR-3L-1.5 with more EB-CFRP layers (Table 3). The axial displacement also increased as the aspect ratio decreased. For instance, it increased from 13.5 mm in STR-3L-1.5 to 14.3, 16.9, and 22.4 mm in STR-3L-1.4, STR-3L-1.3, and STR-3L-1.0, respectively. It can be concluded that the displacement response for confined specimens was mainly governed by the EB-CFRP rigidity and the specimen's elliptical aspect ratio rather than the concrete axial resistance f'_c.

Figure 9 presents the response of load capacity versus axial displacement for each of the aspect ratios (A/B) considered. The figure shows that regardless of the A/B, the control specimens featured an elastic phase up to the ultimate load P_{max} followed by a brittle rupture thereafter. For the series with the same aspect ratio, the load as well as the vertical displacement increased significantly as the confinement increased. The curves for confined specimens show a proportional increase with the number of CFRP layers. Note that the curves have the same tendency and feature two typical linear phases: the first is elastic

from launching the loading until reaching P_{max} of the control specimen, announcing the beginning of the second phase. This behavior reveals that in the first phase, the resistance was governed by the concrete until the ultimate strain ε_{cu} (concrete crushing) was reached, after which, EB-CFRP confinement was effectively activated.

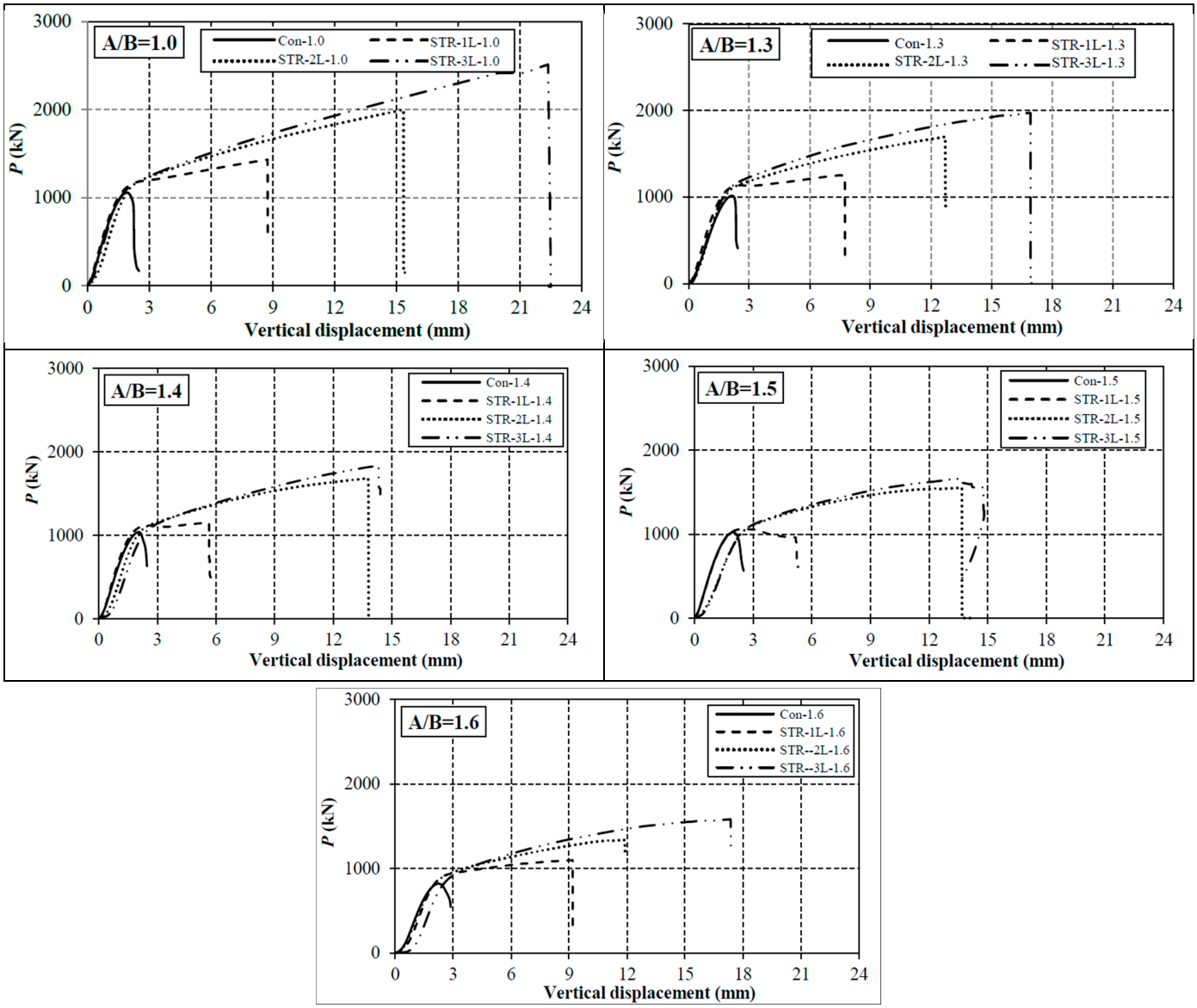

Figure 9. Load versus axial displacement curves for all specimens by aspect ratio (A/B) series.

The second phase, also linear and elastic, started from concrete crushing and continued until CFRP fracture, which corresponded to the maximum load achieved by the specimen. Compared to the first phase, the slope of the second phase was gradual, but it featured a considerably longer plateau up to the abrupt failure of the specimen. The change in the slope angle of the second phase is explained by a change in specimen stiffness, which obviously corresponds to the activation of the EB-CFRP confinement mechanism. This corresponds perfectly to the typical linear behavior until the tensile fracture of the FRP material. Furthermore, observation of the second phase made it possible to conclude that confinement considerably enhances the ductility of a specimen, especially as the number of EB-CFRP layers increases (Figure 9).

Comparing results in terms of the aspect ratio (A/B), Figure 9 shows a decrease in both P_{max} and the corresponding vertical displacement when the aspect ratio A/B increases. This

clearly indicates that the confinement efficiency decreases from the circular to the elliptical section. For instance, the maximum load P_{max} and the vertical displacement, (2513 kN) and (22.4 mm), respectively, of the circular specimen (A/B = 1.0) STR-3L-1.0 decreased in the elliptical specimen (A/B = 1.6) STR-3L-1.6 to 1582 kN and 17.4 mm, respectively. Note that the influence of an increase in aspect ratio was extremely penalizing. A 37% loss in P_{max} from circular- to elliptical-confined specimens with aspect ratio A/B = 1.6 was observed. This can be attributed to the fact that confinement effectiveness depends on column section shape. The distribution of confinement pressure f_{lF} is uniform in a circular column (A/B = 1.0), which means that this section is perfectly confined. However, when the aspect ratio is greater than 1.0 (elliptical column), the confining pressure is not well distributed around the section, creating unconfined zones. Nevertheless, all confined specimens ruptured by fracture of the CFRP material, meaning that the latter reached its ultimate limit, ε_{FRPU}. However, the non-uniform tensile force in the fibers in the elliptical specimens explains the cause of fracture at the maximum pressure zone.

5.4. Compressive Strength Analysis

Figure 10 presents the axial stress versus axial displacement of unconfined control column specimens. The axial stress (compressive strength) was obtained by dividing the maximum load P_{max} by the specimen cross-sectional area with the assumption that the load was uniformly distributed. The curves of all specimens featured very similar trends in the elastic phase until the maximum axial stress, with a slight decrease in the Con-1.6 specimens. The curves shown in Figure 10 are very similar and are typical stress–strain curves of normal concrete in compression. This indicates that the different cross-sections of elliptical columns do not affect the axial stress of unconfined concrete columns, as can be seen in Table 3 and Figure 11. This can be proved by the fact that for the control specimens, the difference was 10% in the compressive strength and around 0.4 mm in the axial displacement (between specimens Con-1.0 and Con-1.6). In contrast, for the confined specimens with three CFRP layers, the differences were around 30% in compressive strength and 5 mm in axial displacement (Figures 10 and 11 and Table 3).

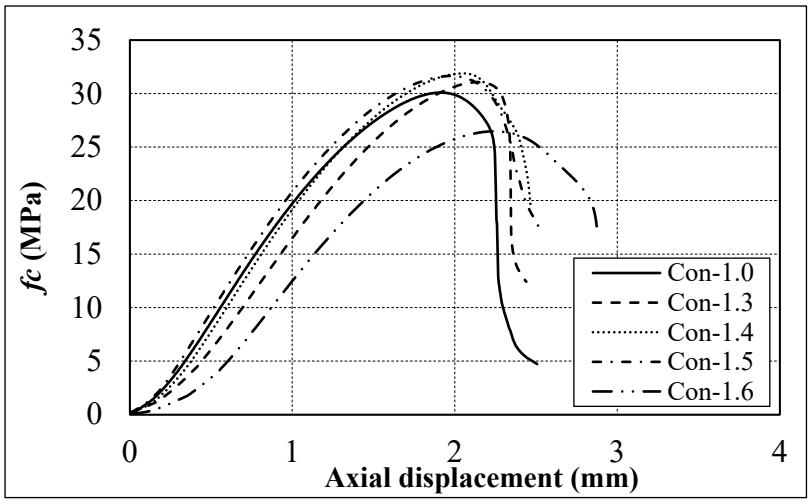

Figure 10. Compressive strength in control specimens.

Figure 12 illustrates the compressive stress–strain curves for aspect ratio A/B = 1.0. This figure clearly reveals the improvement in compressive strength due to confinement with EB-CFRP increasing as reinforcement rigidity increases. The curves of the confined specimens show a considerable increase in compressive strength (f'_{cc}), in axial strain, and, hence, in ductility. In fact, the gain due to three EB-CFRP layers in the circular specimen STR-3L-1.0 was 137% with respect to the corresponding control specimen Con-1.0, although the compressive strain was substantially larger in the confined specimen than in the control

one. Moreover, the curves of the confined specimens followed almost the same trends and were governed by their enhanced elasticity and ductility response. This was evidenced by the considerable branch in the second phase of the three confined specimens compared to the corresponding control one. Figure 12 also shows an increase in the rigidity of the confined specimen as the number of layers increased. Therefore, it can be concluded that the compressive strength of confined concrete evolves in proportion to the number of EB-CFRP layers.

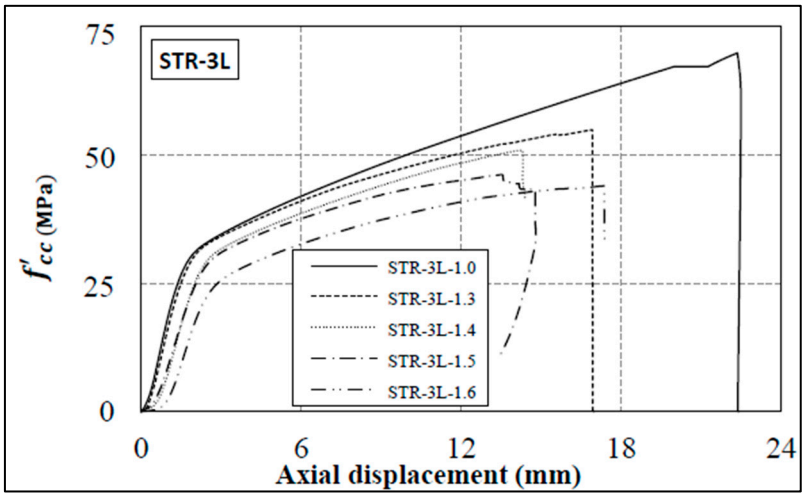

Figure 11. Compressive strength in confined specimens with 3 EB-CFRP layers.

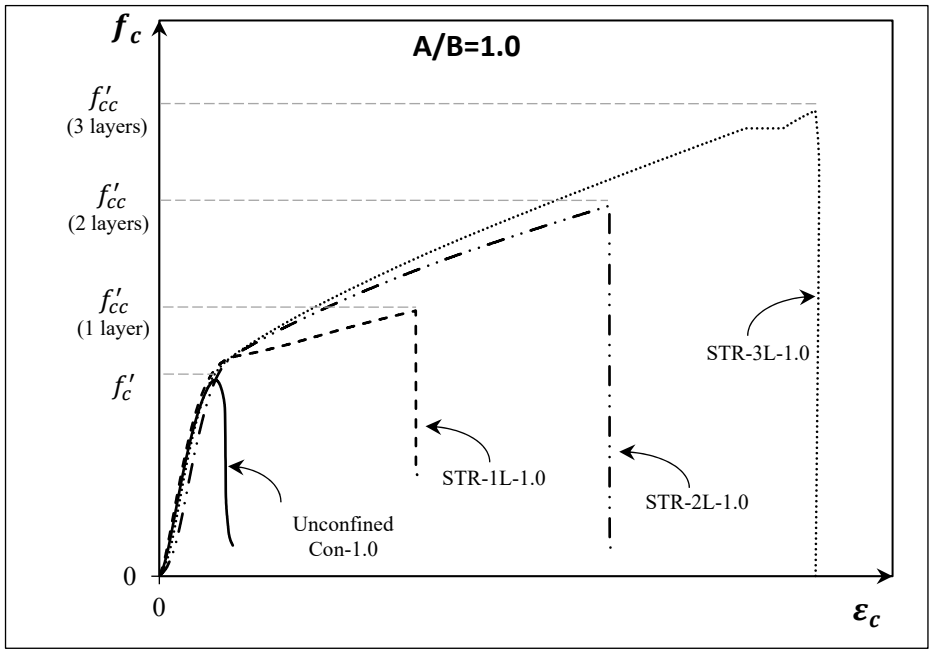

Figure 12. Compressive strength in the aspect ratio A/B = 1.0 series.

5.5. Stress–Strain Behavior

The maximum attained strain values reached at the peak of compressive strength in the horizontal direction (hoop strain) or in the vertical one (axial strain) for all specimens are provided in Table 3. The measured strain distribution curves are presented in Figure 13. Note that deformation in the horizontal direction was in tension due to concrete expansion, which explains its positive value in Figure 13. The deformation in the vertical direction was negative due to compression and shortening of the concrete column in the axial

direction. Table 3 indicates that the strain generally increased in both directions of the confined specimens with the increasing rigidity of EB-CFRP (number of layers). Note that all confined specimens had a monotonically ascending stress–strain curve, which is similar to the results reported in the literature by Teng and Lam [12] and Teng et al. [17]. Figure 13 shows that the CFRP strain (hoop or vertical) was higher when the specimen had a circular form (A/B = 1.0) and always decreased as the aspect ratio (A/B) increased. In addition, strains in both directions evolved proportionally with CFRP jacket rigidity. In fact, the average value of hoop strain in the elliptical specimen confined with one CFRP layer was 12,700 µm/m. This average strain increased to 15,000 and 16,200 µm/m in specimens with two and three EB-CFRP layers, respectively. This result can be attributed to the high level of pressure around the cross-section by the confinement, which is proportional to CFRP thickness. When the latter increased, the circumferential pressure increased and prevented lateral concrete expansion, thereby increasing the tension in the CFRP jacket and hence the hoop strain.

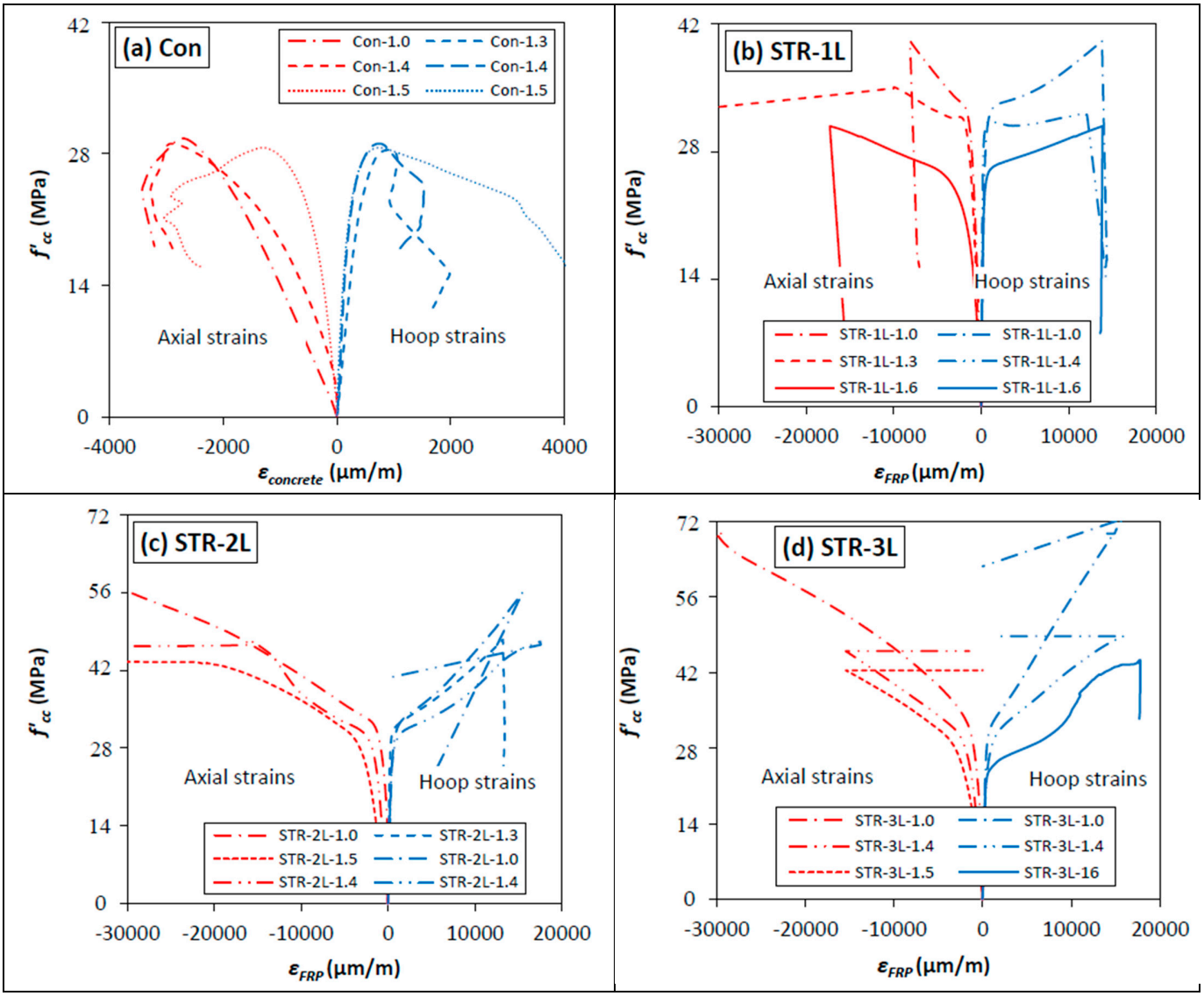

Figure 13. Stress–strain curves in all specimens' series: (**a**) control series (Con); (**b**) confined with one CFRP layer (STR-1L); (**c**) two CFRP layers (STR-2L); and (**d**) three CFRP layers (STR-3L).

5.6. Hoop Strain Analysis

Figure 14 illustrates the distributions of hoop strain for different positions around the cross-section, as mentioned earlier in the instrumentation description. This includes all confined specimens with various aspect ratios (A/B) presented in terms of the number of EB-CFRP layers. The distributions of the hoop strain in each specimen are presented for several significant load levels to obtain an insightful analysis of specimen behavior with special emphasis on the concentration of the confining pressure around the cross-section. In these figures, the vertical axis represents the hoop strain gauge reading, and the horizontal axis represents the position of the gauge. The latter was designated by the circumferential angle of the elliptical cross-section with respect to the position of the strain gauge H1 corresponding to 0°, as shown in Figure 6. Note that in some specimens of Figure 14, the load levels were not the same because they showed significant variations in hoop strain up to the maximum load (100%). Note that results in some specimens are not shown due to malfunctions of the corresponding strain gauges. Figure 14 shows the maximum hoop strain attained at failure P_{max} in most specimens approaching the ultimate EB-CFRP strain ε_{FRPu} given by the manufacturer's property data sheet (Table 2).

Teng et al. [17] stated that when the confined column section is circular, the confining pressure provided by a uniform EB-FRP sheet f_{lF} is uniformly distributed around the cross-section. However, in an elliptical column, the pressure distribution becomes asymmetric and leads to a decrease in EB-FRP effectiveness. Note that the result from this study is different from those observed by Teng et al. [17] and by Teng and Lam [12]. The latter stated that the maximum strain measured on the CFRP jacket at rupture is significantly lower than the ultimate strains measured from flat coupon tests or from the manufacturer's property data sheet.

In the present study, the authors believe that the location zone of the CFRP fracture in each specimen represents the cause of the specimen failure, given that this zone coincides with the maximum hoop strain reached around the cross-section (Figure 14). The zone also corresponds to the maximum pressure around the cross-section, even if the fracture occurs only on one side. There is no relation between the symmetrical cross-section and the supposed identical pressure distribution at opposite vertices of the elliptical section. This phenomenon can be attributed to concrete surface imperfections or uneven EB-CFRP application, particularly for three CFRP layers, where a very highly one-sided concentration of the hoop strain was observed (Figure 14).

Figure 14 shows that the hoop strain distribution in circular specimens with an aspect ratio of A/B = 1.0 was more uniform, regardless of the number of EB-CFRP layers, than in elliptical specimens. Moreover, the hoop strain curves corresponding to different load levels are almost parallel, which indicates that the EB-CFRP was perfectly bonded to the concrete surface in circular specimens. The hoop strain distribution seemed to be uniform for low load levels (50% and 80%) when confinement was applied with one EB-CFRP layer. These strains then increased with increasing load levels. When the number of EB-CFRP layers was increased, the hoop strain showed a rapid increase with applied load. At 80% of maximum load, the CFRP strain attained, approximately, half the ultimate CFRP strain ε_{FRPu}. Thereafter, the curves of each confined specimen showed an abrupt strain increase somewhere around the specimen circumference. However, the strain increase tended to be concentrated at the major or minor vertex in the other cases. Moreover, the change in hoop strain from a uniform distribution around the circumference specimen to a concentration in the highest lateral pressure zones was related to (a) an increase in the load level and (b) an increase in the elliptical aspect ratio (Figure 14). In addition, Figure 14 shows that in specimens confined with three EB-CFRP layers, only one strain gauge reached the maximum value ε_{FRPu} corresponding to the failure zone exhibited in the specimens. In contrast, in specimens with one and two EB-CFRP layers, the maximum hoop strain value was always accompanied by another hoop strain zone close to the maximum. This can explain the moment of rupture, where specifically the columns confined with three EB-CFRP layers made a loud exploding noise as described above.

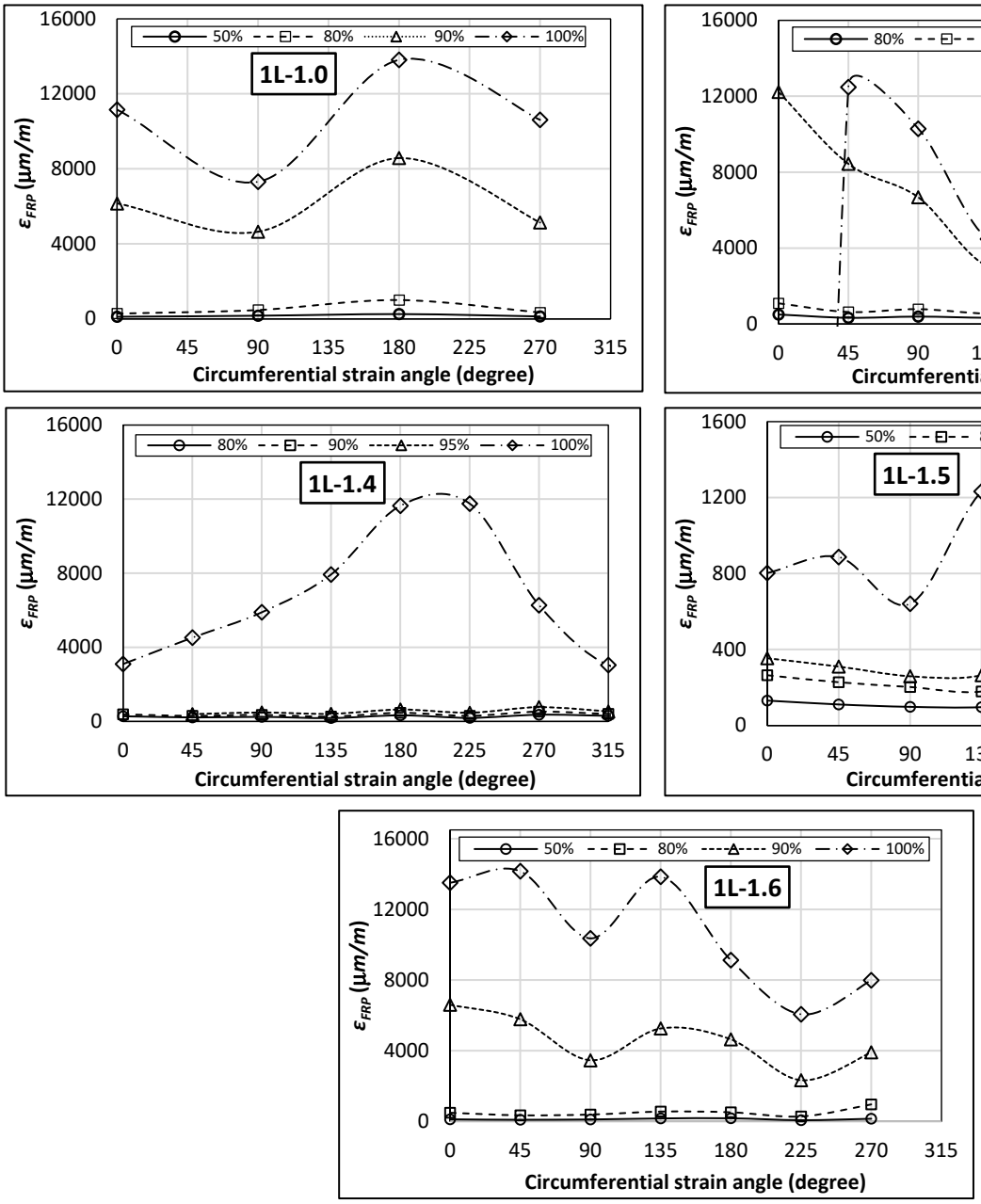

(**a**)

Figure 14. *Cont.*

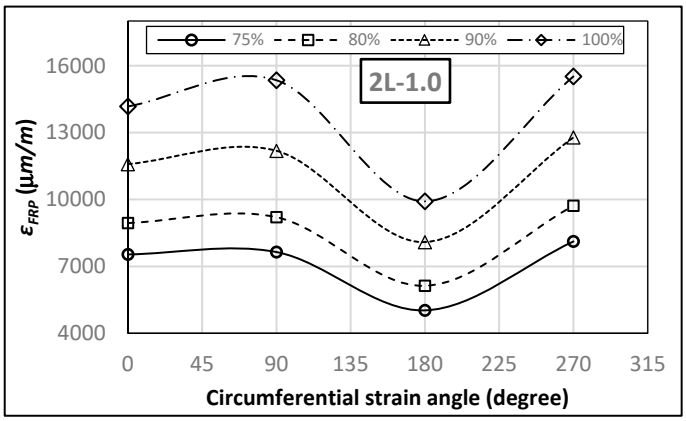

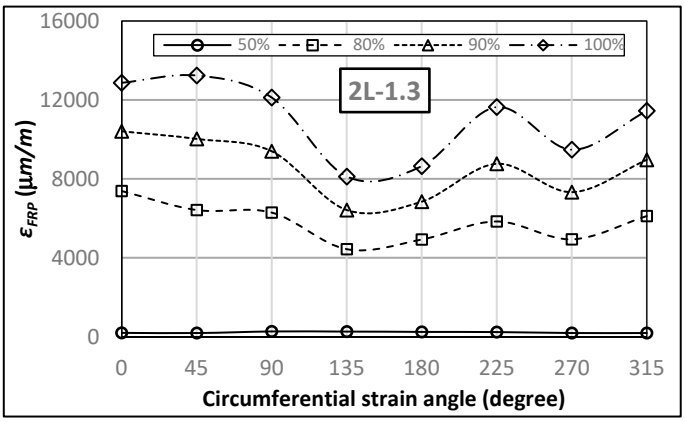

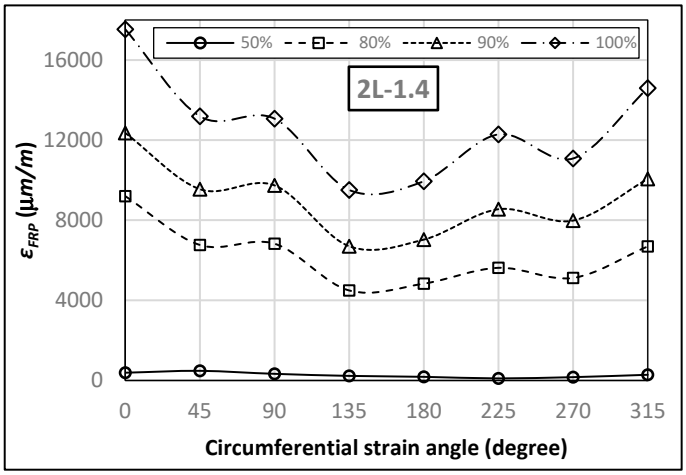

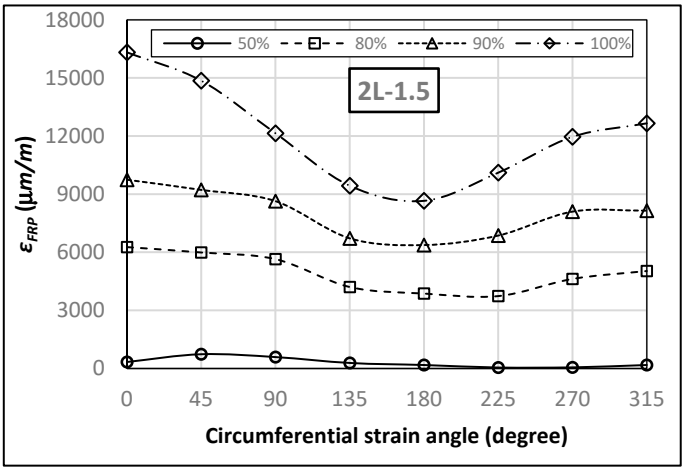

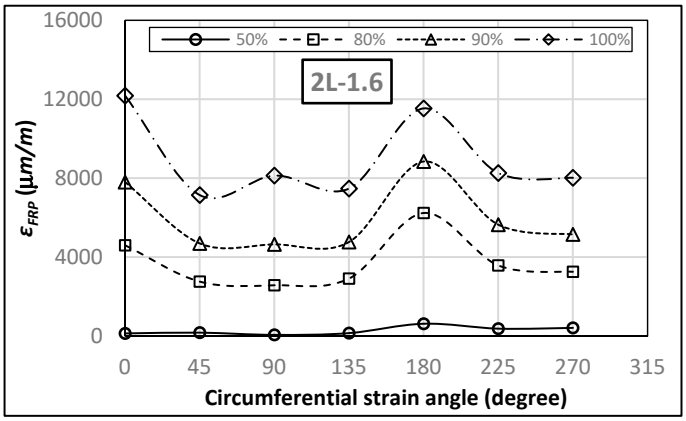

(**b**)

Figure 14. *Cont.*

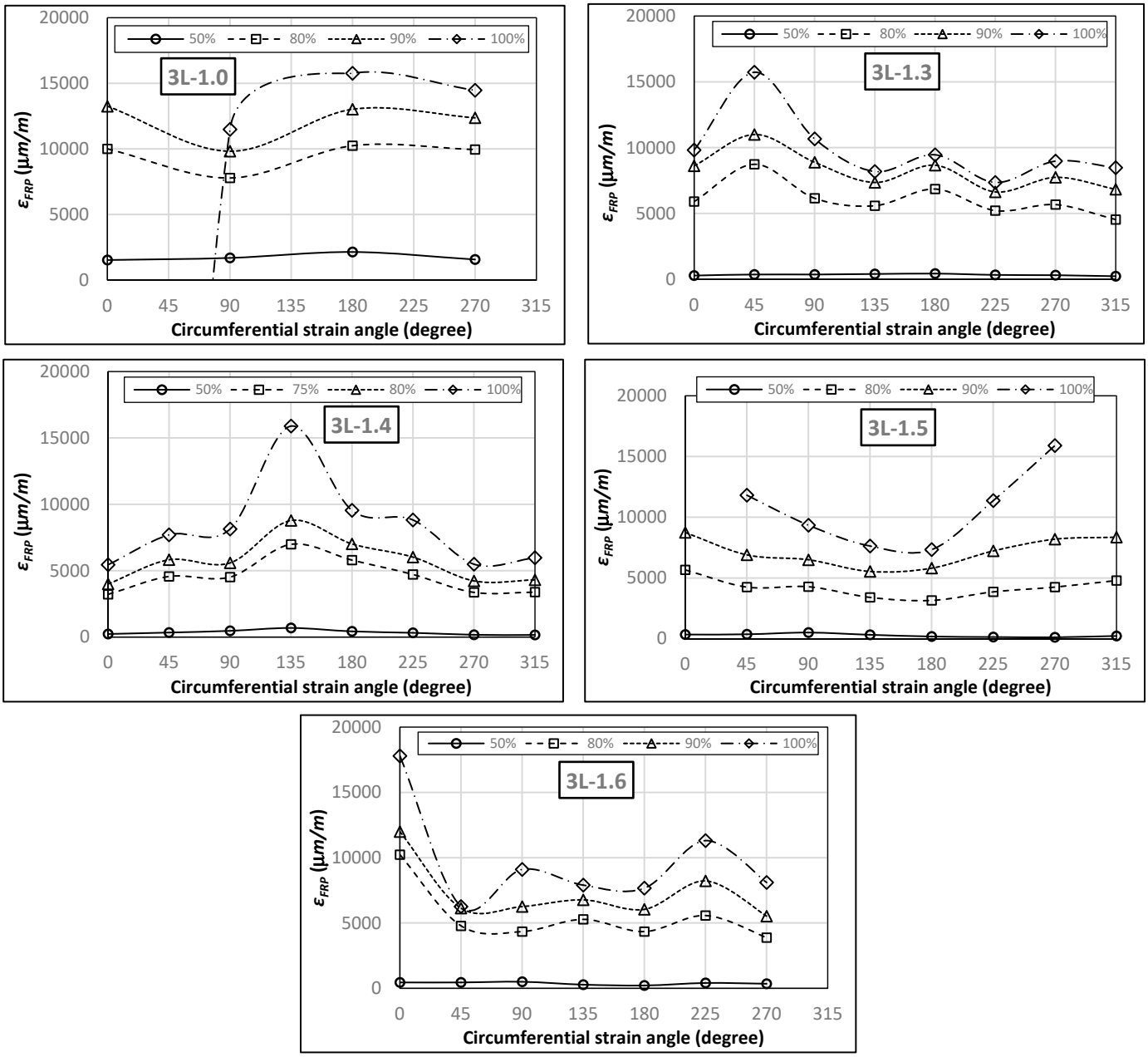

(**c**)

Figure 14. Hoop strain curves around the cross-section: (**a**) specimens with one CFRP layer; (**b**) specimens with two CFRP layers; and (**c**) specimens with three CFRP layers.

5.7. Compressive Strength Accuracy Prediction Code

To better understand the influence of the aspect ratio in an elliptical cross-section, Figure 15 illustrates the compressive strength achieved by the confined specimens expressed with respect to the circular specimen compressive strength ($f'_{cc(A/B)}/f'_{cc(1.0)}$). To evaluate the accuracy of the predictive models, Figure 15 includes the ratio of compressive strength for all confined specimens as well as their corresponding values as predicted by the CSA-S806-21 [35] and CSA-S6-19 [36] using Equations (2) and (4), respectively. The data for confined series with an aspect ratio of A/B = 1.6 were not included in this sensitive comparison with model codes because the results were inconsistent, as explained before. The curves of the experimental test results showed a significant strength reduction when increasing the aspect ratio. In contrast, the code curves revealed no change in compressive strength with elliptical aspect ratio, according to the CSA-S6-19 [36] prediction.

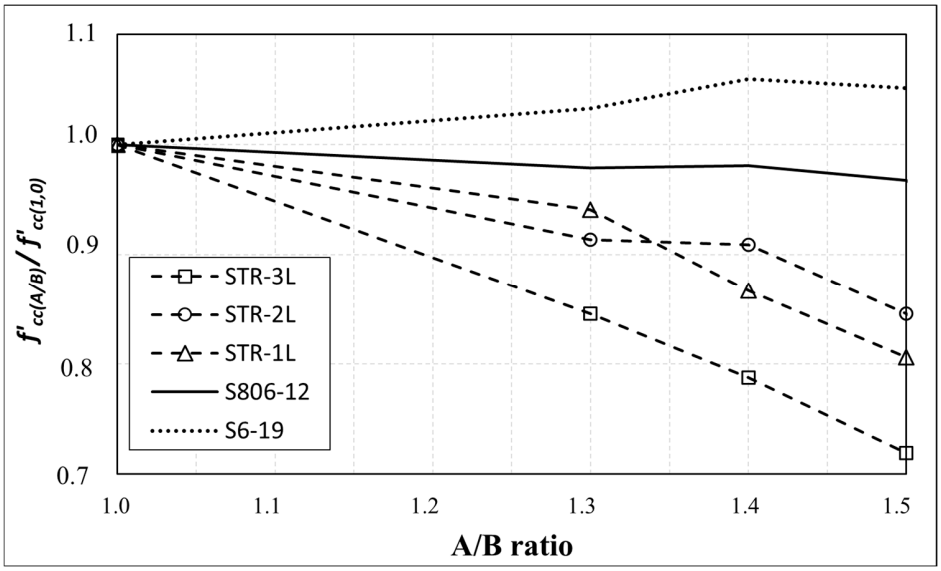

Figure 15. Relative compressive strength in confined specimens: model codes versus experimental results.

Indeed, the compressive strength values of the circular specimens (A/B = 1.0) was identical, in most cases, to those of the elliptical specimens, regardless of the aspect ratio according to the CSA-S806-21 [35] curve. In addition, Figure 15 shows an inversely proportional relationship between compressive strength and elliptical aspect ratio. In other words, the decrease in compressive strength from the test results with respect to the circular specimen was amplified as the rigidity of EB-CFRP confinement increased. It can be concluded that the prediction models used by the standards fail to capture the effect of the aspect ratio for elliptical-confined specimens. In fact, the impact of increasing the elliptical aspect ratio is a reduction in EB-CFRP's effectiveness on the confined column. Therefore, until these important parameters are captured, these models should be used with caution.

6. Conclusions

The external strengthening of elliptical concrete columns confined with externally bonded carbon fiber-reinforced polymer (EB-CFRP) laminates is a technique implemented to strengthen RC columns of buildings and bridges. This study investigated the influence of the elliptical aspect ratio in confined concrete columns as a function of different EB-CFRP layers. The following two parameters were considered: (1) the aspect ratio, A/B; and (2) the number of EB-CFRP layers. The results showed that the effectiveness of EB-CFRP laminates is directly related to the aspect ratio and to CFRP rigidity. The predictive accuracy of the Canadian standards in terms of confinement effectiveness was also assessed. The main findings of this study are as follows:

- Increasing the CFRP rigidity by providing additional CFRP layers considerably enhances the columns' compressive strength as well as the displacement. The maximum increase in ultimate strength was 130%. The displacement was governed by the aspect ratio (A/B) of the specimens rather than by the compressive strength of concrete, f'_c. Furthermore, the aspect ratio A/B can considerably affect the effectiveness of EB-CFRP confinement, which decreases as the aspect ratio (A/B) increases.
- The failure mode of all confined specimens was by fracture of the CFRP laminates. This failure occurred after concrete crushing, which indicates that CFRP laminates can remain operational and contribute to ultimate strength in spite of concrete crushing.
- CFRP hoop and axial strains increased in the confined specimens with respect to the control specimens with the increase in CFRP rigidity. The strains were higher in circular specimens (A/B = 1.0) and decreased with the increase in the aspect ratio of elliptical specimens.

- The hoop strain changed from a uniform distribution around the specimen circumference to non-uniform in elliptical specimens. In this case, the highest hoop strain concentrated in the lateral pressure zones depending on (a) the increase in the load level and (b) the increase in the aspect ratio (A/B).
- The predictive models used by the Canadian standards did not capture the effect of the aspect ratio for elliptical confined columns. In fact, the model codes simply associated the circular cross-sectional behavior for the elliptical one in terms of pressure stress distribution around the cross-section. The current design guidelines should be modified when more experimental and numerical data are available.

Author Contributions: Conceptualization, O.C.; Methodology, Z.E.A.B. and O.C.; Formal analysis, Z.E.A.B., O.C. and A.G.; Investigation, Z.E.A.B., O.C. and A.G.; Data curation, Z.E.A.B., O.C. and A.G.; Writing—original draft, Z.E.A.B., O.C., A.G. and R.A.H. Review—A.G. and O.C. All authors have read and agreed to the published version of the manuscript.

Funding: This research was financially supported by the Natural Sciences and Engineering Research Council of Canada (NSERC) and the Fonds de recherche du Québec—Nature et technologie (FRQNT) through operating grants. The financial support of the Deanship of Research and Graduate Studies (DRG) at Ajman University is gratefully acknowledged.

Data Availability Statement: Some or all data, models, or codes that support the findings of this study are available from the corresponding author on reasonable request.

Acknowledgments: The authors thank Sika-Canada, Inc. (Pointe Claire, Quebec) for contributing to the cost of materials. The efficient collaboration of Jonathan Auger at École de technologie supérieure (ÉTS) in conducting the tests is acknowledged.

Conflicts of Interest: We declare that we do not have any commercial or associative interest that represents a conflict of interest in connection with the work submitted.

References

1. Liu, F.; Wang, Y.; Chan, T.-m. Behaviour of concrete-filled cold-formed elliptical hollow sections with varying aspect ratios. *Thin-Walled Struct.* **2017**, *110*, 47–61. [CrossRef]
2. Mohamed, S.; Toutanji, H.; Li, Z. Behavior of concrete columns confined with fiber reinforced polymer tubes. *Mater. J.* **1999**, *96*, 500–509.
3. Yan, Z.; Pantelides, C. Concrete column shape modification with FRP shells and expansive cement concrete. *Constr. Build. Mater.* **2010**, *25*, 396–405. [CrossRef]
4. Chen, G.; Wang, Y.; Yu, T.; Wan, B.; Zhang, B.; Liu, Q. Behavior and design-oriented model for elliptical FRP-confined concrete under axial compression. *Eng. Struct.* **2021**, *249*, 113387. [CrossRef]
5. Ismail, R.; Rashid, R.S.M.; Zakwan, F.A.A.; Ahmad, H.; Hejazi, F. Axial behaviour of strengthened circular hollow reinforced concrete column with CFRP partial confinement. *Acta Polytech. CTU Proc.* **2022**, *33*, 250–255. [CrossRef]
6. Liu, K.; Jiang, C.; Yu, T.; Teng, J. Compressive behaviour of elliptical FRP tube-confined concrete columns. *Compos. Struct.* **2022**, *303*, 116301. [CrossRef]
7. Chen, G.; Wang, Y.; Yu, T.; Zhang, B.; Han, B. Elliptical FRP–Concrete–Steel Double-Skin Tubular Columns: Axial Behavior, Interaction Mechanism, and Modeling. *J. Compos. Constr.* **2022**, *26*, 04022078. [CrossRef]
8. Zhang, Q.; Wei, Z.-Y.; Gu, X.-L.; Yang, Q.-C.; Li, S.-Y.; Zhao, Y.-S. Confinement behavior and stress–strain response of square concrete columns strengthened with carbon textile reinforced concrete (CTRC) composites. *Eng. Struct.* **2022**, *266*, 114592. [CrossRef]
9. Zhang, Q.; Yang, Q.; Gu, X.; Jiang, Y.; Zhu, H.Y. Study on the confinement properties of circular concrete columns wrapped with prefabricated textile reinforced fine concrete (TRC) shells. *Front. Struct. Civ. Eng.* **2023**, *17*, 1554–1570. [CrossRef]
10. Zhang, Q.; Yang, Q.; Gu, X.; Jiang, Y. Study on axial compression properties of concrete columns wrapped with basalt textile-reinforced fine concrete (BTRC) jackets. *Constr. Build. Mater.* **2023**, *363*, 129809. [CrossRef]
11. Rochette, P.; Labossiere, P. Axial testing of rectangular column models confined with composites. *J. Compos. Constr.* **2000**, *4*, 129–136. [CrossRef]
12. Teng, J.G.; Lam, L. Compressive behavior of carbon fiber reinforced polymer-confined concrete in elliptical columns. *J. Struct. Eng.* **2002**, *128*, 1535–1543. [CrossRef]
13. Chaallal, O.; Hassan, M.; LeBlanc, M. Circular columns confined with FRP: Experimental versus predictions of models and guidelines. *J. Compos. Constr.* **2006**, *10*, 4–12. [CrossRef]
14. Youssef, M.N.; Feng, M.Q.; Mosallam, A.S. Stress–strain model for concrete confined by FRP composites. *Compos. Part B Eng.* **2007**, *38*, 614–628. [CrossRef]

15. Pham, T.M.; Doan, L.V.; Hadi, M.N. Strengthening square reinforced concrete columns by circularisation and FRP confinement. *Constr. Build. Mater.* **2013**, *49*, 490–499. [CrossRef]
16. Benzaid, R.; Mesbah, H.-A. The confinement of concrete in compression using CFRP composites–effective design equations. *J. Civ. Eng. Manag.* **2014**, *20*, 632–648. [CrossRef]
17. Teng, J.; Wu, J.; Casalboni, S.; Xiao, Q.; Zhao, Y. Behavior and modeling of fiber-reinforced polymer-confined concrete in elliptical columns. *Adv. Struct. Eng.* **2016**, *19*, 1359–1378. [CrossRef]
18. Hadi, M.N.S.; Jameel, M.T.; Sheikh, M.N. Behavior of circularized hollow RC columns under different loading conditions. *J. Compos. Constr.* **2017**, *21*, 04017025. [CrossRef]
19. Zeng, J.-J.; Guo, Y.-C.; Gao, W.-Y.; Li, J.-Z.; Xie, J.-H. Behavior of partially and fully FRP-confined circularized square columns under axial compression. *Constr. Build. Mater.* **2017**, *152*, 319–332. [CrossRef]
20. Jameel, M.T.; Sheikh, M.N.; Hadi, M.N. Behaviour of circularized and FRP wrapped hollow concrete specimens under axial compressive load. *Compos. Struct.* **2017**, *171*, 538–548. [CrossRef]
21. Obaidat, A.T.; Ashteyat, A.M.; Obaidat, Y.T.; Al-Btoush, A.Y.; Hanandeh, S. Experimental and numerical study of strengthening and repairing heat-damaged RC circular column using hybrid system of CFRP. *Case Stud. Constr. Mater.* **2021**, *15*, e00742. [CrossRef]
22. Obaidat, Y.; Barham, W.; Obaidat, A.; Attar, K. Behavior of NSM CFRP reinforced concrete columns: Experimental and analytical work. *Case Stud. Constr. Mater.* **2021**, *15*, e00589. [CrossRef]
23. Ali, R.; Shafiq, M.A.; Zakwan, F.A.A.; Ahmad, H.; Ismail, R.; Ismail, B.N. Compressive strength and behaviour of full and partial CFRP confined concrete columns. *ESTEEM Acad. J.* **2022**, *18*, 41–54.
24. Ashteyat, A.; Obaidat, A.; Obaidat, Y.; Al-Tarawneh, D. The behavior of strengthened and repaired RC columns with (CFRP) rope under different preloading levels. *Eur. J. Environ. Civ. Eng.* **2023**, *27*, 4212–4236. [CrossRef]
25. Gambarelli, S.; Nisticò, N.; Ožbolt, J. Numerical analysis of compressed concrete columns confined with CFRP: Microplane-based approach. *Compos. Part B Eng.* **2014**, *67*, 303–312. [CrossRef]
26. Wang, J.; Shen, Q.; Jiang, H.; Pan, X. Analysis and design of elliptical concrete-filled thin-walled steel stub columns under axial compression. *Int. J. Steel Struct.* **2018**, *18*, 365–380. [CrossRef]
27. Cai, Y.; Quach, W.-M.; Young, B. Experimental and numerical investigation of concrete-filled hot-finished and cold-formed steel elliptical tubular stub columns. *Thin-Walled Struct.* **2019**, *145*, 106437. [CrossRef]
28. Ali, O.; Abbas, A.; Khalil, E.; Madkour, H. Numerical investigation of FRP-confined short square RC columns. *Constr. Build. Mater.* **2021**, *275*, 122141. [CrossRef]
29. Fan, L.; Jin, L.; Du, X. Modeling of size effect on compressive behavior of CFRP-confined rectangular RC columns: Influence of corner radius and aspect ratio. *Compos. Struct.* **2022**, *304*, 116400. [CrossRef]
30. Pan, J.; Xu, T.; Hu, Z. Experimental investigation of load carrying capacity of the slender reinforced concrete columns wrapped with FRP. *Constr. Build. Mater.* **2006**, *21*, 1991–1996. [CrossRef]
31. Zhu, J.Y.; Lin, G.; Teng, J.-G.; Chan, T.-M.; Zeng, J.-J.; Li, L.-J. FRP-confined square concrete columns with section curve linearization under axial compression. *J. Compos. Constr.* **2020**, *24*, 04020004. [CrossRef]
32. Zeng, J.J.; Teng, J.G.; Lin, G.; Li, L.J. Large-scale FRP-confined rectangular RC columns with section curvilinearization under axial compression. *J. Compos. Constr.* **2021**, *25*, 04021020. [CrossRef]
33. *CNR-DT200R1*; Guide for the Design and Construction of Externally Bonded FRP Systems for Strengthening Existing Structures. CNR-DT200R1-13; National Research Council: Roma, Italy, 2013.
34. *fib-TG9.3-19*; Externally Bonded FRP Reinforcement for RC Structures. fib TG9.3-01 Bulletin 14. Fédération Internationale du Béton: Lausane, Switzerland, 2019.
35. *CSA-S806-21*; Règles de calcul et de construction des structures de bâtiment contenant des polymères renforcés de fibres. Norme CAN/CSA S806-12. Canadian Standards Association: Mississauga, ON, Canada, 2021.
36. *CSA-S6-19*; Canadian Highway Bridge Design Code. Norme CAN/CSA S6-19. Canadian Standards Association: Mississauga, ON, Canada, 2019.
37. *ASTM-C39/39-18*; Standard Test Methods for Compressive Strength of Cylindrical Concrete Specimens. ASTM C39/39-18. American Society for Testing Materials: West Conshohocken, PA, USA, 2018.